All-fiber spectral filtering with solid core photonic band gap Bragg fibers

Alexandre Dupuis, Ning Guo, Bertrand Gauvreau,
Alireza Hassani, Elio Pone, Francis Boismenu,
Maksim Skorobogatiy

École Polytechnique de Montréal, Génie Physique, C.P. 6079, succ. Centre-Ville
Montreal, Québec H3C3A7, Canada
www.photonics.phys.polymtl.ca

Abstract: We report on intensely colored solid core all-polymer Bragg fibers, with a large diameter PMMA core surrounded by alternating PMMA/PS layers. Modifying reflector layer thickness illustrates that bandgap position can be adjusted in the visible.
© 2007 Optical Society of America

OCIS codes: 060.2280 Fiber design and fabrication; 060.2270 Fiber characterization; 999.9999 Solid core Bragg fibers

1. Introduction

Microstructured plastic optical fibers have been recently applied to various important problems including data communication over short distances [1, 2, 3]; non-linear optics [4]; light amplification[5]; sensors [6, 7, 8]; as well as mid-IR [9] and THz guiding [10, 11].

In this letter, we present fabrication and optical characterization of a solid-core photonic crystal all-polymer Bragg fiber for guiding in the visible range. The fiber is designed in a view of its potential applications in plasmonic fiber-based sensors [7], high bandwidth datacom links [3], as well as in color-selective illumination.
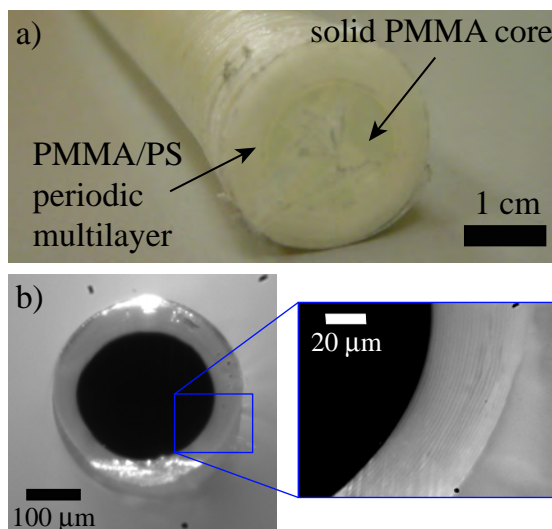
Fig. 1. a) Bragg fiber preform featuring solid PMMA core and a 50 layer PMMA/PS reflector. b) Optical micrograph of the drawn fiber cross-section.

2. Fabrication and measurements

The fibers detailed in this letter consist of a large PMMA core surrounded with a 50-layer PMMA/PS Bragg reflector of refractive index contrast ∼ 1.49/1.59. A co-rolling process [12] was used to make the fiber preform. Large bandgaps (spectral width of up to ∼ 25% of a bandgap center wavelength) were predicted [13] for this material combination. Fibers with distinct realizations of photonic bandgaps were fabricated by drawing the same preform into fibers of various outside diameters [14].

Details of the fabrication process are as follows. The fiber preform (Fig. 1(a)) was prepared using commercial plastic rods and films. Particularly, PMMA film was purchased from the Degussa company; PS film was purchased from the Dow Chemical Company; PMMA rods were purchased from McMaster Carr Canada.

The core consisted of a 1.27cm diameter PMMA rod which was degassed and annealed in an oven at 90°C for 48 hours prior to use. PS and PMMA films, both of 50 μm thickness, were then co-rolled around a PMMA core rod to create 50 alternating PS/PMMA layers (Bragg reflector). The fiber preform was consolidated in an oven at 130°C for 4 hours. The preform was then mounted in a draw tower and preheated at 150°C for 2 hours. The fiber was subsequently drawn at 180°C at a speed of 1000 mm/min. Figure 1(b) shows a microscope image of the fiber cross-section with Bragg reflector layers clearly visible.

The fiber was drawn from the same preform down to several different diameters, ranging from 100 to 350 μm, with an aim of varying the spectral position of the photonic bandgap. Transmission through ∼20cm of such fibers was then studied using a supercontinuum white-light source focused by an objective into the fiber center. Observation of the fibers revealed that upon launching white light, all its spectral components not guided by the reflector bandgap were irradiated in the first 1-3 cm along the fiber length. Subsequently, only a particular color guided by the bandgap was propagated to the fiber end (Fig. 2). Moreover, due to imperfections, side-scattering loss in such fibers is substantial, thus leading to coloring of the whole fiber by the guided color.
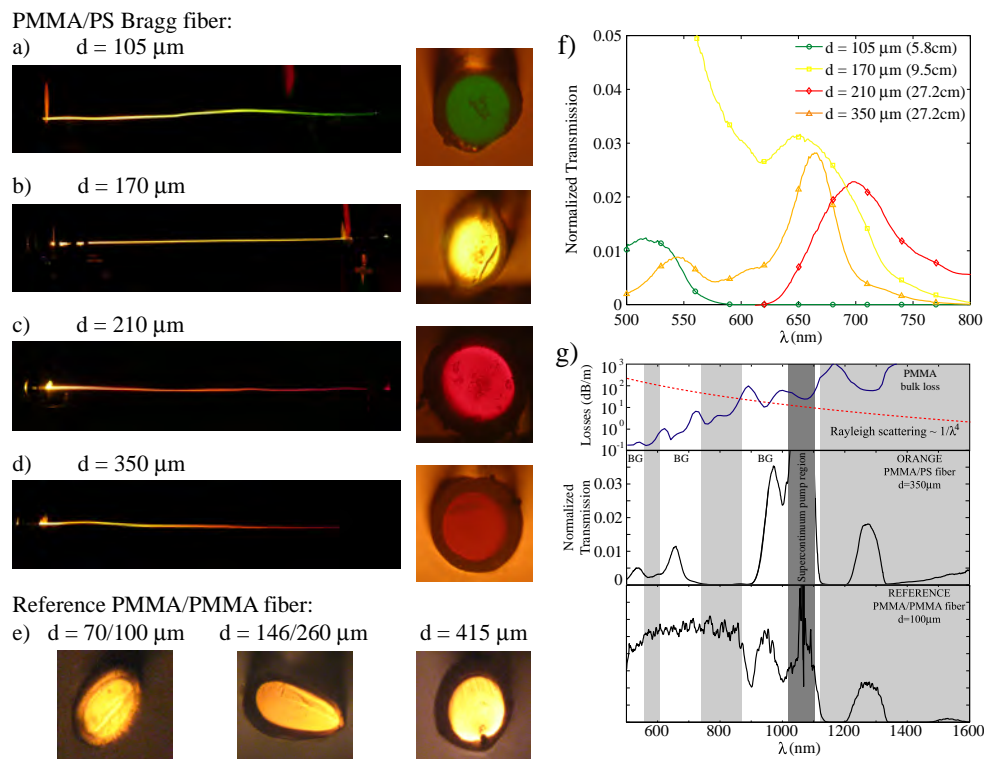
Fig. 2. Photographs of the side-scattered and transmitted light for fibers of different diameters. White light beam from a supercontinuum source was focused by an objective and launched into the fiber center. (a)-(d) PMMA/PS Bragg fiber, (e) Reference PMMA/PMMA fiber. Furthermore, normalized transmission spectra of fibers of different diameters are presented are on the right. (f) Visible spectra. (g) Visible and near-IR spectra for a 350 μm diameter PMMA/PS Bragg fiber and a a 100 μm diameter PMMA/PMMA reference fiber.

The fiber photonic bandgaps were then independently observed by recording the fiber transmission spectra with the aid of a monochromator. Fig. 2(f) presents the fiber transmission spectra in the visible region normalized by the power spectrum of a supercontinuum source. Fiber segments having outside/core diameters of 350/250, 210/145, 170/103, 105/77 μm guide reddish-orange, red, yellow and green light respectively. The corresponding fiber lengths studied were respectively 27.2, 27.2, 9.5, and 5.8 cm. It is worth noting that the human perception of color is quite complex. Thus, for example, while the spectral transmission peak of the 350 μm diameter fiber is at red (660 nm), the actual color perceived by the eye is orange due to the presence of a second peak in the green (540nm). Overestimate of the solid-core Bragg fiber losses from the corresponding normalized spectra give 0.6-4 dB/cm fiber loss depending on the sample. As we will show later, the main contribution to such loss in the near-IR is a PMMA absorption loss, while in the visible it

is scattering off the fiber imperfections, which, in principle, can be greatly reduced through perfecting the preform fabrication process. Simulations of the fiber transmission properties revealed that all the fibers are guiding by the higher order photonic bandgaps.

3. Discussion

Interpretation of the spectra in Fig. 2(f) is not trivial as several loss mechanisms are contributing simultaneously. A detailed discussion on the interpretation of the spectra can be found in [15]. As an example, we discuss the shape of the transmission spectrum, in Fig. 2(g), of a Bragg fiber with diameter of $350\mu m$. In the near-IR region above 1000nm, all the spectral peaks can be explained by the shape of the PMMA material loss curve alone, with transparency windows in material loss resulting in enhanced fiber transmission in their vicinity of 950, 1050, and 1300nm. Below 1000nm, we expect Rayleigh scattering off fiber imperfections. In the upper part of Fig. 2(g) we present a Rayleigh scattering curve (dotted) having functional form $70[dB/m] \cdot (660nm/\lambda[nm])^4$. Parameters of this functional form were chosen to fit the amplitude of a spectral peak at 660nm.

In order to demonstrate that PMMA absorption and Rayleigh scattering are insufficient to explain all the structural features of the Bragg fiber transmission spectra in the visible, we fabricated a reference fiber made entirely of PMMA. To more faithfully reproduce the type of fiber non-uniformities that arise during the fabrication method of the Bragg fiber, we opted to roll a PMMA film around a PMMA rod and to draw the resulting structure. The PMMA film and the PMMA rod were the same as those used for the PMMA/PS Bragg fiber. The PMMA reference fiber was drawn to different diameters ranging from 100 μm to 415 μm, see Fig. 2(e). All these fibers scattered and transmitted light that appeared orange to the naked eye and had similar transmission spectra. We attribute the guidance in the PMMA core to a slight refractive index difference with respect to the PMMA film that was used for the cladding. The transmission spectrum of a PMMA reference fiber of 70/100 μm diameter and 12.9 cm in length is presented in Fig. 2(g) and can be explained by considering the above-mentioned PMMA absorption and Rayleigh scattering. With only these two loss mechanisms present, one expects a relatively featureless spectrum in the visible, and a transmission maximum around 800-900nm.

In conclusion, we demonstrated bandgap guidance in solid-core Bragg fibers operating in a visible range. Bandgap position was adjusted by drawing fibers of different outside diameters, and various colors coming out of the fibers were recorded when excited with a white light source. Fiber losses in the near-IR are dominated by the PMMA material loss, while in the visible they are dominated by scattering off reflector imperfections.

3. References

1. Y. Koike, T. Ishigure, and E. Nihei, J. Light. Technol. **13**, 1475 (1995).
2. M.A. van Eijkelenborg, A. Argyros, A. Bachmann, G. Barton, M.C.J. Large, G. Henry, N.A. Issa, K.F. Klein, H. Poisel, W. Pok, L. Poladian, S. Manos, and J. Zagari, Elec. Lett. **40** (2004).
3. M. Skorobogatiy, N. Guo, Opt. Lett. **32**, 900 (2007).
4. D. W. Garvey, K. Zimmerman, P. Young, J. Tostenrude, J. S. Townsend, Z. Zhou, M. Lobel, M. Dayton, R. Wittorf, M. G. Kuzyk , J. Sounick, and C. W. Dirk, J. Opt. Soc. Am. B **13**, 2017 (1996).
5. K. Kuriki, Y. Koike, and Y. Okamoto, Chem. Rev. **102**, 2347 (2002).
6. C.M.B. Cordeiro, M.A.R. Franco, G. Chesini, E.C.S. Barreto, R. Lwin, C.H. Brito Cruz, and M.C.J. Large, Opt. Express **14**, 13056 (2006).
7. A. Hassani, M. Skorobogatiy, J. Opt. Soc. Am. B **24**, 1423 (2007).
8. L. Rindorf, P.E. Hoiby, J.B. Jensen, L.H. Pedersen, O. Bang, and O. Geschke, Analyt. Bioanalyt. Chem. **385**, 1370 (2006).
9. G. Dellemann, T.D. Engeness, M. Skorobogatiy, and Uri Kolodny, Phot. Spectra **37**, 60 (2003).
10. H. Han, H. Park, M. Cho, and J. Kim, Appl. Phys. Lett. **80**, 2634 (2002).
11. M. Skorobogatiy, A. Dupuis, Appl. Phys. Lett. **90**, 113514 (2007).
12. Y. Gao, N. Guo, B. Gauvreau, M. Rajabian, O. Skorobogata, E. Pone, O. Zabeida, L. Martinu, C. Dubois, and M. Skorobogatiy, J. Mat. Research **21**, 2246 (2006).
13. M. Skorobogatiy, Opt. Lett. **30**, 2991 (2005).
14. E. Pone, C. Dubois, N. Guo, S. Lacroix, and M. Skorobogatiy, J. Light. Techn. **24**, 4991 (2006).
15. A. Dupuis, N. Guo, B. Gauvreau,, A. Hassani, E. Pone, F. Boismenu, and M. Skorobogatiy, Opt. Lett., to be published.